Published in final edited form as:
Stroke. 2010 October ; 41(10 Suppl): S21–S25. doi:10.1161/STROKEAHA.110.595066.

Endoluminal Scaffold for Vascular Reconstruction and Exclusion of Aneurysms from the Cerebral Circulation

Baruch B. Lieber, PhD and **Chander Sadasivan, PhD**
Stony Brook University, Department of Neurological Surgery, Stony Brook, NY 11794

Abstract

The latest class of neuro-endovascular devices being evaluated is intended to treat cerebral aneurysms. Besides inducing flow stasis mediated thrombosis of aneurysms, and thus at times referred to as flow diverters, these devices reconstitute pathological arterial segments to near-physiological normalcy. The successful implementation of such an endoluminal scaffold for vascular reconstruction (ESVR) in the cerebral circulation requires a careful consideration of various factors drawn from engineering, physics and biological sciences. Here we review some of these factors.

Keywords

Aneurysms; Hemodynamics; Angiography; Animal Models

Engineering an ESVR

The key engineering issues in the manufacturing of a neuro-endovascular device such as an endoluminal scaffold for vascular reconstruction (ESVR) are the choice of materials, design of the construct and manufacturing methods e.g., laser-cutting vs braiding or knitting. A priori knowledge of biocompatibility limits the choice to a small number of materials from a very large arsenal of alloys. Further, the construct needs to have the mechanical stability and strength to provide enough outward radial force to remain in the implanted location without migrating while providing superior apposition to the luminal wall of highly tortuous of cerebral vessels. It is also desirable to make the device of one type of material to avoid galvanic corrosion over time. Given these constraints, we have selected a Cobalt-Chromium alloy that is widely used as surgical implant material due to its biocompatibility, excellent fatigue properties, high corrosion resistance, and mechanical strength [1,2]. It also exhibits kink resistance and flexibility and its extruded wire form is used to weave the ESVR. Our experience with the use of this material in the elastase-induced aneurysm model in rabbit has been very favorable [3] with no undesirable acute (or chronic) biological response and preserved structural integrity over the long term.

Porosity

We have evaluated ESVRs composed of wires ranging from 30 to 50 microns in diameter with a variable number of ends (see Figure 1, number of ends designated as N) and various weave

Correspondence: Baruch B. Lieber, HSC T12, Room 080, Stony Brook University Medical Center, Stony Brook, NY 11794-8122, Tel: 631.444.1278, Fax: 631.444.1535, blieber@notes.cc.sunysb.edu.

angles (β) to achieve a nominal porosity index ranging from 65% to 70%. The porosity of the ESVR is defined as:

$$porosity(\%)=\frac{Total\ Surface\ Area\ -\ Metal\ Surface\ Area}{Total\ Surface\ Area}\times 100 \quad (1)$$

The term coverage or cover factor (100 - porosity%) is also occasionally used to represent this parameter. The length of the ESVR should be selected such that the total length (L) spans the width of the aneurysm neck plus at least one and one half of the parent vessel diameter on each side (Δ) to ensure sufficient proximal and distal landing zones to anchor the ESVR in the parent artery. This requirement is balanced with the need to make the device short enough to be able to deliver it through tortuous cerebral arteries and minimize disturbance of the adjacent vessels. Based on our experience and simple geometrical considerations it is possible to easily deliver an ESVR through a catheter with an inner luminal diameter of less than 800 microns.

Pore Density

The porosity of loosely woven ESVRs does not uniquely define the porous medium. Although the pore size could be used as the additional parameter required for uniqueness, the pore size of braided devices changes with changes in the diameter of the device as compared to its stress-free condition. Therefore, we have elected to use the mathematical variable of pore density, which depends on the wire thickness, number of ends and the porosity index. It is essentially the inverse of the area of the opening within each repeatable cell of the device. Figure 2 demonstrates the concept of lack of uniqueness of porosity alone to define a device. In this example if one considers the white diamonds as holes and the black ones as metal, the porosity of the two panels in Figure 2 is the same at 50%. However, the figure on the left has a sixteen fold higher pore density than the one on the right. The concept of pore density, or pore size, is very important for the biological response of the artery to the implant since the pore density determines the properties of the scaffold over which cellular elements proliferate and populate.

Changes in Flow Physics due to an ESVR

We used particle image velocimetry and elastomeric replicas of the elastase-induced aneurysm model in rabbit to investigate flow in the parent artery and within the aneurysm. We investigated six different configurations of ESVRs and studied the influence of the porosity and pore density parameters on the flow field (see Figure 3). Our studies showed a complex interaction between parent vessel flow and intra-aneurysmal flow. This interaction is partially responsible for the replenishment of fresh blood into the aneurysmal sac each heart beat. Thus, the prevailing hemodynamics maintains a good supply of oxygen and nutrients to the pathology. Therefore, decoupling the parent vessel flow from that of the aneurysm is essential for curative remodeling of the pathology and a properly designed ESVR should appropriately modify the local hemodynamics to exclude the pathology from the circulation [4]. We developed four indices of device performance based on well known flow physics. Two of the indices were related to the vorticity function and were reduced to practice by calculating the instantaneous intra-aneurysmal hydrodynamic circulation.

$$\vec{\xi}=\left(\frac{\partial v}{\partial x}-\frac{\partial u}{\partial y}\right)\hat{k} \quad (2a)$$

$$\Gamma = \iint A\vec{\xi} \bullet \vec{n}\, dA \tag{2b}$$

Equation 2a represents the vorticity in the x–y plane with velocity vectors *u* and *v* along the *x* and *y*-axis, respectively. Equation 2b is the hydrodynamic circulation, where *A* is the area of a contour element around which the circulation is calculated and $\vec{n}$ is the vector normal to this element. The selected indices of performance were the peak (which usually occurs during systole) and mean hydrodynamic circulation throughout the cardiac beat.

The next two indices of performance were derived from the instantaneous kinetic energy inside the aneurysmal sac. Again, the peak and mean values of energy throughout the cardiac cycle were evaluated.

$$E = \frac{1}{2}\rho V v^2 \tag{3}$$

Here, *E* is the kinetic energy, ρ is the density, *V* is the volume, and *v* is the velocity. As no changes in volume and density are expected, the square of the velocity alone can be evaluated.

All the ESVRs performed well and significantly reduced the intra-aneurysmal hydrodynamic circulation and energy indices as compared to the control (no device) case (Figure 3). Wall shear stress in the vicinity of the aneurysm neck, which has been implicated in aneurysm growth, was also significantly reduced. The devices reduced the mean hydrodynamic circulation to about 12.5% ± 2.5% of the control and the mean kinetic energy to 21.6% ± 5.8% of that in the control. Devices E and C affected the lowest mean hydrodynamic circulation, mean energy (Figure 3) and peak energy as compared to the others. In summary, devices E and C scored the best results in three of the four indices and almost scored the best in terms of the peak circulation index. Moreover, the change in peak circulation did not reach significance for any of the ESVRs. Thus, it was reasonable to conclude that these particular devices (E and C) would be the best performers in vivo.

We constructed elastase-induced aneurysms in rabbits [5,6] and implanted three different ESVRs. The devices selected were two that scored the best (devices C and E, Figure 3) and device B that had the same porosity but different pore density than device E. Twenty one (n=9), 90 (n=9) & 180 days (n=12) post-implantation, the aneurysms were evaluated by angiography, the animals were sacrificed, and the vasculatures containing the implants were harvested for histological evaluation. Figure 4 shows angiograms acquired before treatment and at 180 day follow-up of an animal treated with device C. As can be noted, the aneurysm has been successfully occluded by the device. The relative performance of the 3 devices as measured purely by the intra-aneurysmal flow reduction indices in vitro was clearly reflected in the aneurysm occlusion rates in vivo [3].

We have also quantified the changes in intra-aneurysmal hemodynamics due to ESVR implantation using angiographic data [7,8]. The aneurysm is delineated as a region of interest and, by defining a position vector to track the aneurysm as it moves, the aneurysmal contrast washout curve is recorded. This washout curve is then fit to the following model, which isolates the convective and diffusive modes of aneurysmal flow exchange.

$$f(t) = \rho_{conv} \int_0^t \frac{1}{\alpha\sqrt{2\pi}} e^{-\frac{(\eta-\mu)^2}{2\sigma^2}} \times \frac{1}{\tau_{conv}} e^{-\frac{t-\eta}{\tau_{conv}}} d\eta + \rho_{diff} \left[\int_0^t \frac{1}{\sigma\sqrt{2\pi}} e^{-\frac{(\eta-\mu)}{2\sigma^2}} d\eta - (1 - e^{-\frac{t}{\tau_{diff}}}) \right] \tag{4}$$

ρ_{conv} and ρ_{diff} represent the relative magnitudes of convective and diffusive transport, respectively, while τ_{conv} and τ_{diff} are the corresponding time constants. The parameters σ and μ characterize the method of contrast injection. Figure 5A shows the washout curves obtained before and immediately after implantation of a device. The marked reduction in amount of contrast entering the aneurysm and its relatively sluggish washout can be noted on this figure. Figures 5B and 5C show the fits of the mathematical model to these two curves. As would be expected, an increase in the amplitude of the diffusive component (ρ_{diff}) and a decrease in the amplitude of the convective component (ρ_{conv}) of the model can be noted. The inset table lists the values of the washout curve amplitudes and optimized values of the three more important model parameters obtained after fitting the pre- and post-implant washout curves. By quantifying the washout of contrast from the aneurysm with these optimized parameters, the performance of various ESVRs can be statistically compared. Also, the optimized time constants were found to have a linear correlation to the mean kinetic energy obtained using particle image velocimetry [9]. Such quantification could also be used to estimate the long-term occlusion potential of the aneurysm immediately after device implantation (while patient is being treated). The inset in Figure 5 shows such an index, called the washout coefficient (*W*). For all the animals combined, a value of this index of less than 30 predicted greater than 97% angiographic occlusion of the aneurysm at follow-up with a sensitivity and specificity of 73% and 82%, respectively [8].

Biological response to an ESVR

We have successfully implanted three configurations of ESVRs with varying porosities and pore densities (65% 14 pores/mm^2, 70% 12 pores/mm^2 and 70% 18 pores/mm^2) across 30 in vivo aneurysms. Device E yielded an angiographic occlusion rate of 97±1% (mean ± standard error of mean for 3 cases) at 21 days with equivalent values at 90 and 180 days. The lower porosity device C, which did not perform well at 90 days follow-up (percentage aneurysm occlusion 62±10%) was able to occlude the aneurysm at 180 days (95±5% occlusion based on 4 cases) [3]. These results suggest that the thrombus deposition in the aneurysm and its conversion to stable scar tissue can be a lengthy process in this species (rabbit), and is much longer than in other experimental aneurysms such as the canine [10] or porcine [11] models.

These findings were confirmed by our histological results, which show that at 21 days follow-up the aneurysm dome is filled with red untransformed thrombus. At 90 days follow-up the thrombus in the aneurysm only starts to show transformation to scar tissue and even at 180 days follow-up, remnants of fresh thrombus are visible. Since the thrombotic and thrombolytic profile of the rabbit is considered close to that of the human [12], it is reasonable to believe that the remodeling process in humans spans a similar period. A recent preliminary evaluation of flow diverters in aneurysm patients also suggests this to be the case [13]. Figure 6A shows an aneurysm section 180 days after implantation of device C. As the devices are designed from thin wires and exert the minimum requisite radial force, they elicit a minimal yet stable neointimal response (Figure 6B); there was no ‘in-stent stenosis’ in any of the implants. Arterial side branches remained patent in all animals at all time points (Figures 6C and 6D).

Acknowledgments

Work supported by NIH under grant number R01NS045753

References

1. Marti A. Cobalt-base alloys used in bone surgery. Injury 2000;31 Suppl 4:18–21. [PubMed: 11270075]
2. Park, JB.; Bronzino, JD., editors. Biomaterials: principles and applications. Boca Raton: CRC Press; 2003. p. 3-5.

3. Sadasivan C, Cesar L, Seong J, Rakian A, Hao Q, Tio FO, Wakhloo AK, Lieber BB. An original flow diversion device for the treatment of intracranial aneurysms: evaluation in the rabbit elastase-induced model. Stroke 2009;40(3):952–958. [PubMed: 19150864]

4. Seong J, Wakhloo AK, Lieber BB. In Vitro Evaluation of Flow Divertors in an Elastase-Induced Saccular Aneurysm Model in Rabbit. ASME J. Biomech. Eng 2007;129(6):863–872.

5. Cesar L, Miskolczi L, Lieber BB, Sadasivan C, Gounis MJ, Wakhloo AK. Neurological deficits associated with the elastase-induced aneurysm model in rabbits. Neurological Research 2009;31(4): 414–419. [PubMed: 18826754]

6. Onizuka M, Miskolczi L, Gounis MJ, Seong J, Lieber BB, Wakhloo AK. Elastase-Induced Aneurysms in Rabbits: Effect of Post-Construction Geometry on Final Size. AJNR Am J Neuroradiol 2006;27(5): 1129–1131. [PubMed: 16687557]

7. Lieber BB, Sadasivan C, Gounis MJ, Seong J, Miskolczi L, Wakhloo AK. Functional Angiography. Crit Rev Biomed Eng 2005;33(1):1–102. [PubMed: 15777157]

8. Sadasivan C, Cesar L, Seong J, Wakhloo AK, Lieber BB. Treatment of rabbit elastaseinduced aneurysm models by flow diverters: development of quantifiable indices of device performance using digital subtraction angiography. IEEE Transactions on Medical Imaging 2009;28(7):1117–1125. [PubMed: 19164085]

9. Trager A, Sadasivan C, Seong J, Lieber BB. Correlation between angiographic and particle image velocimetry quantification of flow diverters in an in vitro model of elastase-induced rabbit aneurysms. Journal of Biomechanical Engineering 2009;131(3):034506. [PubMed: 19154077]

10. Wakhloo AK, Schellhammer F, de Vries J, Haberstroh J, Schumacher M. Self-expanding and balloon-expandable stents in the treatment of carotid aneurysms: an experimental study in a canine model. AJNR Am J Neuroradiol 1994 Mar;15(3):493–502. [PubMed: 8197946]

11. Turjman F, Massoud TF, Ji C, Guglielmi G, Vinuela F, Robert J. Combined stent implantation and endosaccular coil placement for treatment of experimental wide-necked aneurysms: a feasibility study in swine. AJNR Am J Neuroradiol 1994 Jun;15(6):1087–1090. [PubMed: 8073977]

12. Heilman CB, Kwan ES, Wu JK. Aneurysm recurrence following endovascular balloon occlusion. J Neurosurg 1992 Aug;77(2):260–264. [PubMed: 1625015]

13. Lylyk P, Miranda C, Ceratto R, Ferrario A, Scrivano E, Luna HR, Berez AL, Tran Q, Nelson PK, Fiorella D. Curative endovascular reconstruction of cerebral aneurysms with the pipeline embolization device: the Buenos Aires experience. Neurosurgery 2009 Apr;64(4):632–642. [PubMed: 19349825]

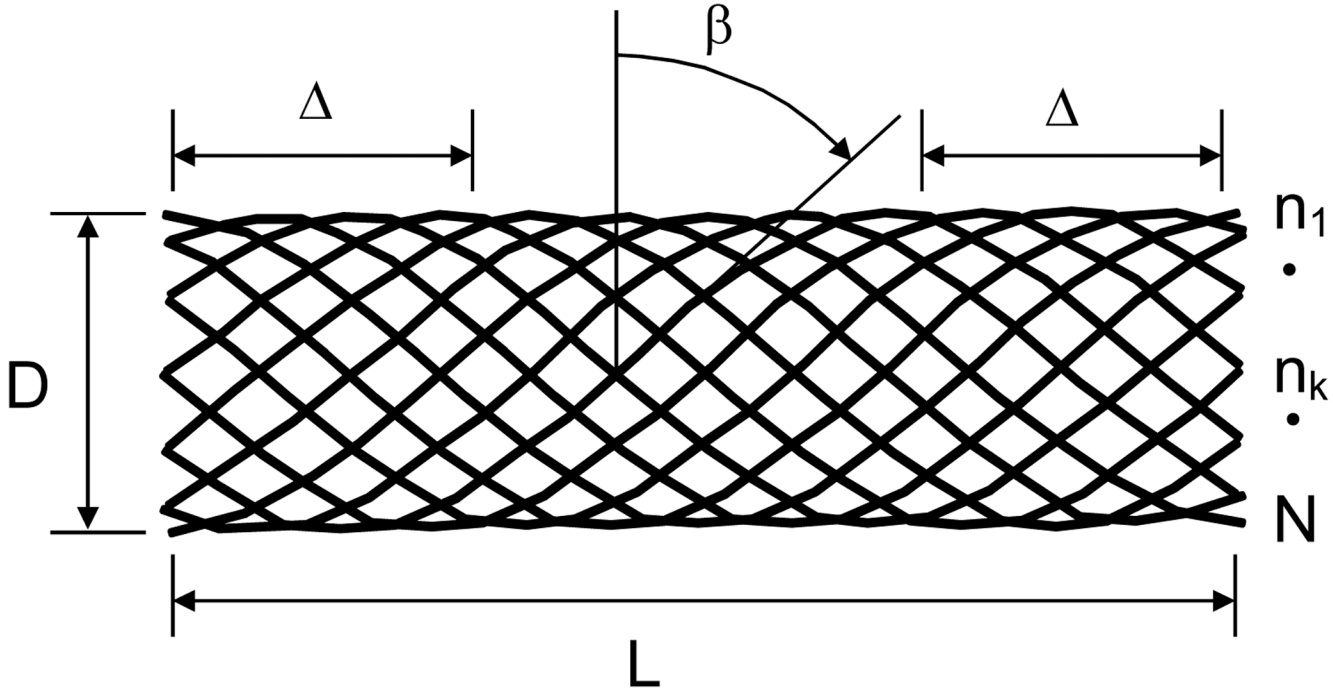

Figure 1.
Schematic of an ESVR. L: device length; D: device diameter; Δ: length of landing zone required to anchor device in parent vessel; β: weave angle; n_1 through N: number of ends

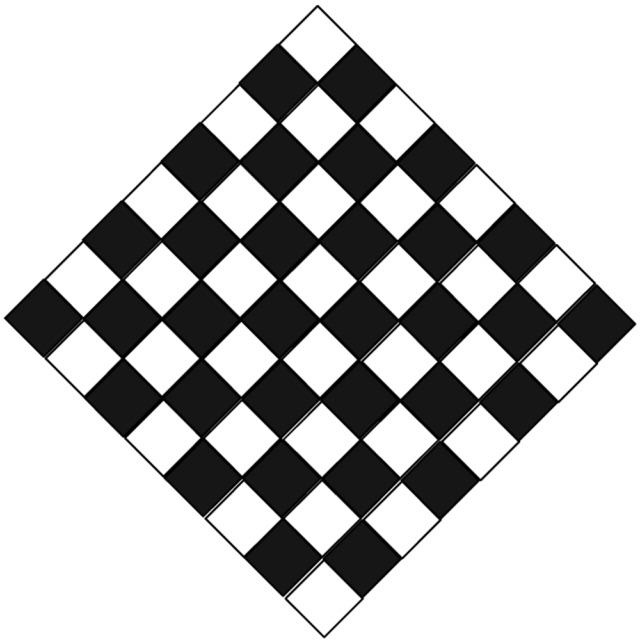

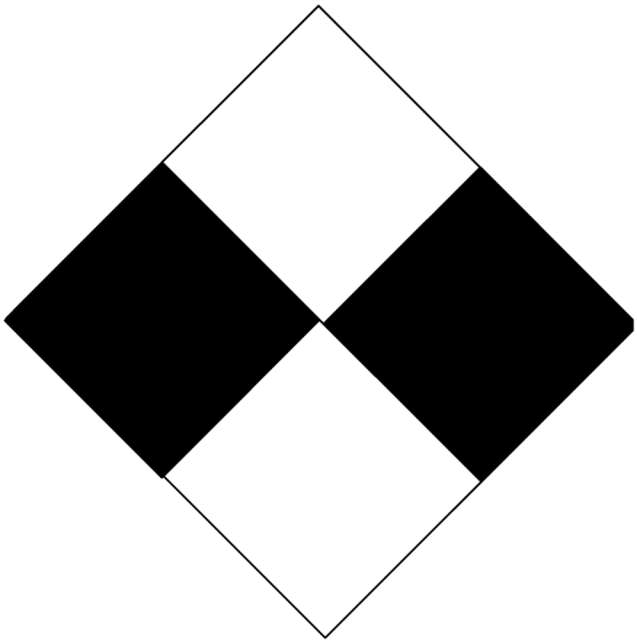

Figure 2.
Equal porosities but different pore densities

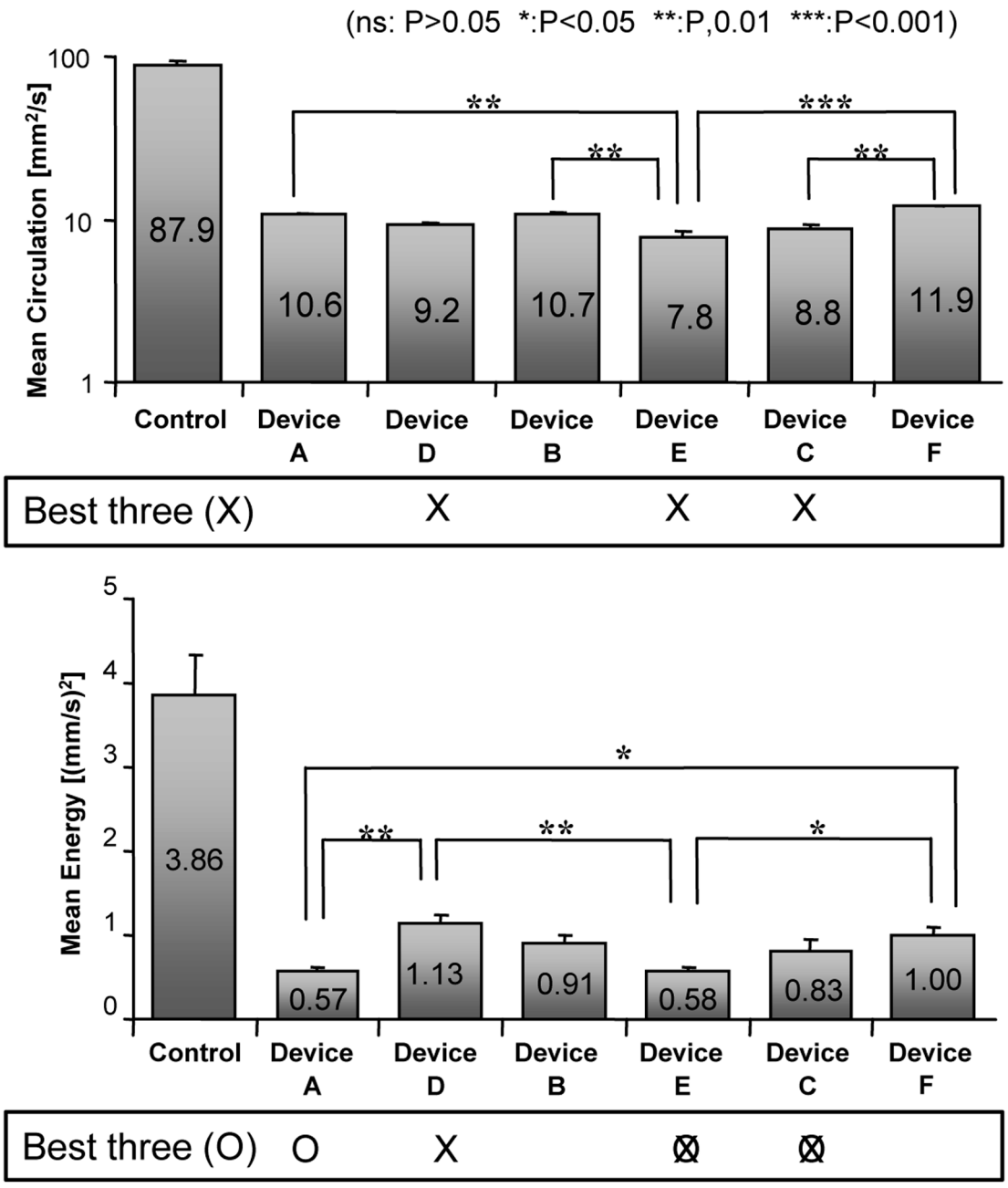

Figure 3.
Mean hydrodynamic circulation and mean energy inside the aneurysm before and after implantation of the device. Error bars denote standard error of mean (n=3) [4]. Crosses and zeros below the plots mark the three best devices for each index.

Figure 4.
(A) In vivo saccular aneurysm before treatment with an ESVR; (B) angiogram at 180 day follow-up shows aneurysm to be completely occluded.

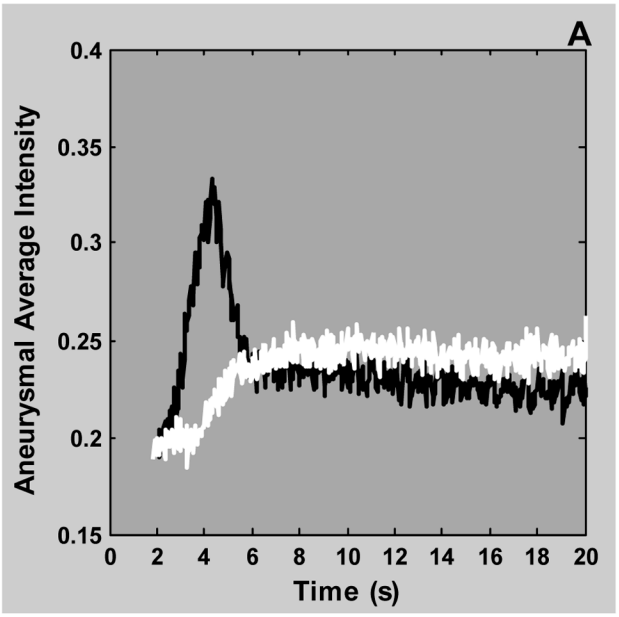

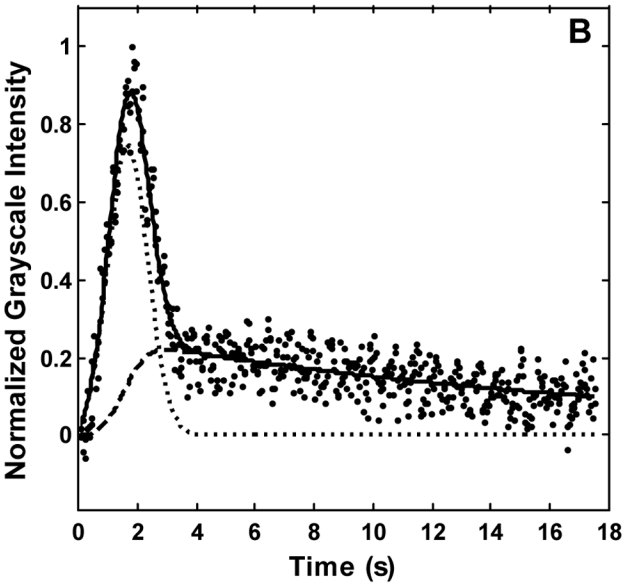

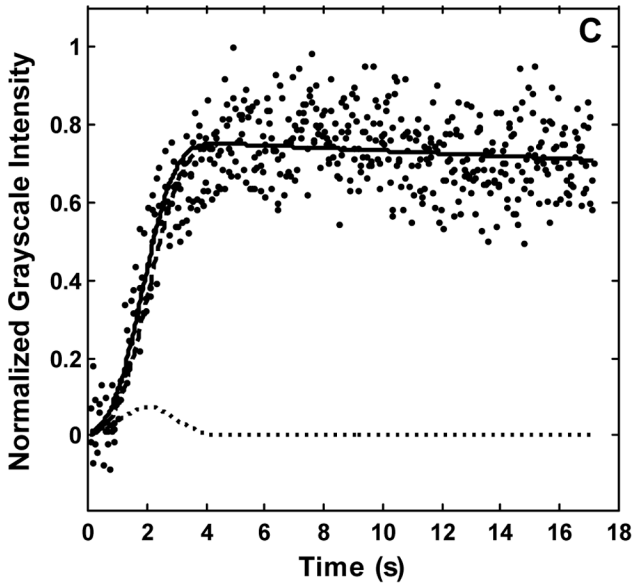

Optimized values of relevant parameters

Angiography	ρ_{conv} (%)	ρ_{diff} (%)	τ_{diff} (s)	Δ
Pre-	77.1	22.9	18.3	0.12
Post-	8.9	91.0	222.1	0.06

δ: intensity, amplitude of washout curve

$$W = \frac{\delta^{POST}}{\delta^{PRE}} \times \frac{\rho_{diff}^{POST}}{\rho_{diff}^{PRE}} \times \frac{\tau_{diff}^{POST}}{\tau_{diff}^{PRE}} = 24$$

Figure 5.

(A) Aneurysmal washout curves obtained before (black line) and immediately after (white line) implantation of a low porosity device. Corresponding model-fits (solid lines) for the pre- (B), and post- (C) washout curves (dotted lines). The convective (dash-dot lines) and diffusive (dash lines) components of the model are also indicated. Inset shows optimized values of some of the model parameters and the washout coefficient (*W*) for this case. Data correspond to Figure 4

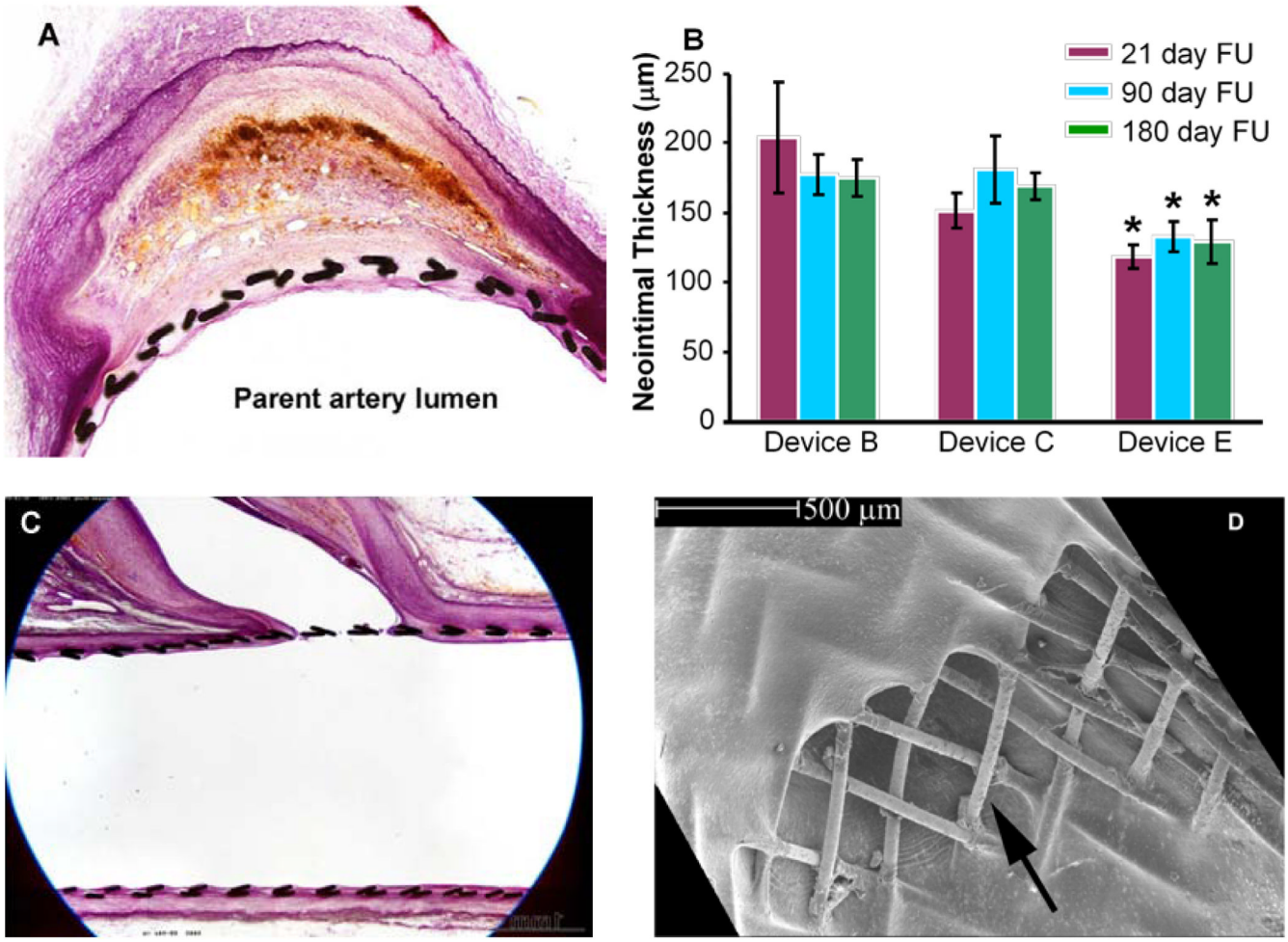

Figure 6.

A) histological section at 180 days shows near-complete fibrosis of aneurysm sac; device struts can be seen to be incorporated by a neointimal layer. B) neointimal thicknesses with the three ESVRs evaluated; * significant difference ($p<0.05$) compared to the other devices; bars represent standard error of the mean. C) and D) side-branch ostia jailed by devices remain patent 180 days after implantation; arrow in panel D shows direction of flow into branch